Interface structure and stabilization of metastable B2-FeSi/Si(111) studied with low-energy electron diffraction and density functional theory

2003 J. Phys.: Condens. Matter 15 5207

(http://iopscience.iop.org/0953-8984/15/30/303)

INSTITUTE OF PHYSICS PUBLISHING JOURNAL OF PHYSICS: CONDENSED MATTER

J. Phys.: Condens. Matter **15** (2003) 5207–5221 PII: S0953-8984(03)59943-X

Interface structure and stabilization of metastable B2-FeSi/Si(111) studied with low-energy electron diffraction and density functional theory

S Walter[1], F Blobner[1], M Krause[1], S Müller[1], K Heinz[1] and U Starke[1,2]

[1] Lehrstuhl für Festkörperphysik, Universität Erlangen-Nürnberg, Staudtstraße 7, D-91058 Erlangen, Germany
[2] Max-Planck-Institut für Festkörperforschung, Heisenbergstraße 1, D-70569 Stuttgart, Germany

E-mail: kheinz@fkp.physik.uni-erlangen.de

Received 24 February 2003
Published 18 July 2003
Online at stacks.iop.org/JPhysCM/15/5207

Abstract

We present a combined experimental and theoretical investigation of the interface between a B2-type FeSi film and Si(111). Using an ultra-thin B2-FeSi film grown on Si(111), the interface is still reached by electrons, so quantitative low-energy electron diffraction (LEED) could be applied to determine the bonding geometry experimentally. As a result, the local configuration at the shallow buried interface is characterized by near-substrate Fe atoms being 8-fold coordinated to Si atoms and by the silicide unit cell being rotated by 180° with respect to the Si unit cell (B8 configuration). The interface energetics were explored by total-energy calculations using density functional theory (DFT). The B8-type interface proves to be the most stable one, consistent with the experimental findings. The atomic geometries obtained experimentally (LEED) and theoretically (DFT) agree within the limits of errors. Additionally, the calculations explain the stabilization of the B2 phase, which is unstable as bulk material: the analysis of the elastic behaviour reveals a reversed energy hierarchy of B2 and the bulk stable B20 phase when epitaxial growth on Si(111) is enforced.

1. Introduction

The growth of iron silicide on a silicon substrate is of considerable technological interest. This is because—dependent on structure and composition—iron silicide can be metallic, semiconducting or ferromagnetic, and therefore offers a large variety of potential applications when integrated into silicon-based devices [1, 2]. Yet it appears that the structure of the growing silicide film can be different from the stable bulk structure for the particular chemical composition chosen. For 1:1 stoichiometry, growth in CsCl-type structure (B2) is observed

instead of the bulk-stable so-called ϵ-FeSi [3], which has the rather complex B20 structure. B2-FeSi is not stable as a bulk structure but—with a lattice mismatch of only 1.5%—grows as a high-quality film on Si(111), as previously reported a decade ago [4] and confirmed repeatedly (e.g. [5–7]). From this work there is some previous knowledge concerning the atomic structure of the films. They are characterized by a low-energy electron diffraction (LEED) pattern showing the same (1×1) periodicity as the (unreconstructed) Si substrate, while the quantitative analysis of diffraction intensities confirms the CsCl structure [7]. Additionally, it could be shown that the film surface is Si-terminated without any ad-layers involved. A rather complicated multilayer relaxation in the surface region—as also determined by quantitative LEED—is reproduced with good agreement by density functional theory (DFT) calculations [7].

Since B2-FeSi is metallic, films on Si are good candidates for Schottky junctions. Yet, to understand the properties of such devices, the crystallography of the interface plays a crucial role. The latter, however, is largely unknown up to now. This holds for the film's orientation relative to the substrate (A or B type, with the unit cells of both materials aligned or mutually rotated by 180°, respectively) as well as for the coordination of the interfacial Fe atoms, which can be 5-, 7- or 8-fold. In the present paper, we address these unresolved issues and determine the atomic structure and energetics of the B2-FeSi/Si(111) interface. We show that quantitative LEED, which is usually considered as only surface sensitive and inapplicable to buried interfaces due to the limited electron penetration, can be applied successfully when the interface is close enough to the surface. Accordingly, we use a particularly thin film of FeSi on top of Si(111)—an approach previously also successful for $CoSi_2$/Si(111) [8]. The atomic geometries retrieved compare well with the results that we obtain from DFT calculations using ultra-soft pseudo-potentials. Additionally, the comparison with theory allows us to illuminate the consequences of the close proximity of the film surface and interface. Also, theory will show that it is through the imposed epitaxial strain that the films grow in B2 (rather than B20) structure and that interface stabilization (suggested earlier [9]) must be ruled out.

2. LEED structure analysis

2.1. Sample preparation, direct structural information and LEED measurements

Film preparation and experiments were carried out in an ultra-high-vacuum (UHV) chamber equipped with reverse-view LEED optics (also used as a retarding-field analyser for Auger electron spectroscopy (AES)) and a beetle-type scanning tunnelling microscope (STM). The samples were heated by electron bombardment from the back. Sample temperatures above 460 °C were measured using an infrared pyrometer; lower temperatures were extrapolated on the basis of the heating power. Iron deposition from an electron beam evaporator was monitored using a quartz microbalance and Auger spectra. As substrate, silicon slices of 7×7 mm^2 in size were cut from a (111)-oriented wafer of 0.5 mm thickness. After standard preparation procedures, it produced a well ordered (7×7) superstructure, as verified by LEED and STM.

The silicide films to be analysed were prepared by deposition of Fe onto Si(111) and subsequent annealing in UHV. For the desired ultra-thin films (two to three silicide layers) this procedure produced films of morphologically better quality than by co-deposition of Si and Fe, as apparent from the STM. This is in spite of the fact that co-deposition turns out to be necessary to produce high-quality thick films [4, 6]. The reason behind this might be that, for ultra-thin films, deposition of only one constituent and subsequent annealing can be much better controlled than stoichiometric co-deposition. For thick films, on the other hand, it requires substantial material transport of iron into the surface, so that, in this case, co-deposition leads

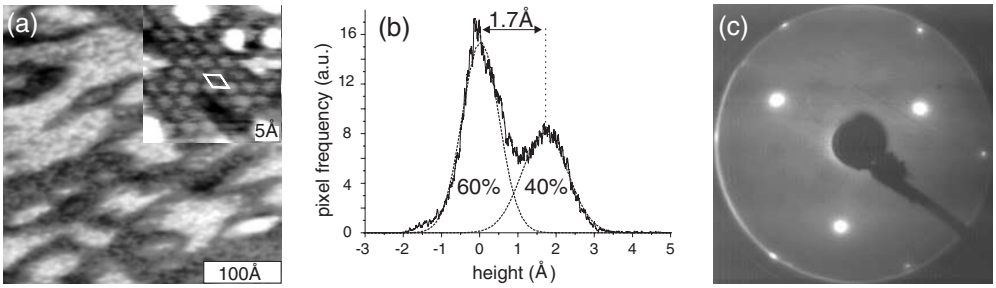

Figure 1. (a) An STM image for (on average) 2.4 silicide layers exhibiting domains of two different heights. In the inset, ($U_{tip} = -1.0$ V) atomic resolution is provided with the real-space unit cell highlighted. (b) An STM histogram of (a) and its evaluation, retrieving both the step height and the domain weights. The smooth curves represent Gaussian fits. (c) A LEED pattern of the same state of the film at 90 eV.

to better films. The LEED spectra for an ultra-thin film prepared by co-deposition are similar to (though not identical to) those of an interface resulting from Fe deposition and subsequent annealing, indicating that the two methods eventually lead to the same type of interface.

Due to the strong reactivity of Fe on Si, even at room temperature no Fe template develops [6, 10]. While the substrate temperature during Fe deposition was rather non-critical (in the range 100–300 K), the film quality was shown to depend sensitively on annealing temperature and time. It was controlled through both the quality of the LEED pattern and the film morphology, as imaged by STM. Figure 1(a) displays the image of a film resulting from the initial deposition of 2.6 ± 0.25 ML Fe and subsequent annealing (one monolayer (ML) of Fe corresponds to one Fe atom per top substrate layer Si atom). The atomically resolved inset in panel (a) allows us to determine the lengths of the unit cell vectors ($\approx$3.8 Å, i.e. coinciding with the value of Si(111)). Obviously, there is layer-by-layer growth, leading to a distribution of domains with two different heights (according to the average coverage being between two and three silicide layers, i.e. two and three pairs of Fe and Si layers). A quantitative evaluation using a Gaussian fit of the histogram shown in figure 1(b) confirms the formation of steps of approximately 1.7 Å in height. Though this evaluation suffers from errors introduced by the background subtraction, the internal structure of the domains and an incomplete fit (estimated error $\approx$0.2 Å), the value of 1.7 Å was confirmed for several STM images. As the layer spacing in B2-FeSi(111) is just about half this value (0.8 Å), there can only be double steps, i.e. the surface must be terminated by either Si or Fe. Integration of the two Gaussian peaks in figure 1(b) gives that $40 \pm 15\%$ of the substrate is covered by the thinner film domain equivalent to an initial Fe coverage of 2.4 ± 0.15 ML, which largely agrees with the less accurate estimation via the quartz balance. The LEED pattern (figure 1(c)) shows the (1×1) periodicity of the (unreconstructed) Si substrate, i.e. for film, interface and substrate (all of them probed by the LEED electrons) the lateral unit cell has the same size and shape.

Intensity versus energy spectra of LEED spots, $I(E)$, were recorded using a fast, video-based data acquisition system [11]. During the measurement, the sample was held at liquid-nitrogen temperature in order to reduce thermal diffuse scattering. Normal incidence of the primary electron beam was adjusted by the comparison of spectra of symmetry-equivalent beams. For the final data-set, the influence of residual misalignment and inhomogeneities of the luminescent screen was further reduced by averaging equivalent spectra. The resulting data-base included seven symmetrically inequivalent beams whose spectra cover a total energy width of $\Delta E = 1981$ eV.

2.2. Intensity calculations and structural search

The computation of the LEED I(E) spectra was performed using the TensErLEED program package [12]. This is based on the tensor LEED perturbation method [13–15], allowing for the fast variation of structural and non-structural parameters. The structure fitting the experimental data best was found by an automated structural search procedure [16], guided by the Pendry R-factor R_P [17]. Error limits were estimated using the variance of the R-factor, $\mathrm{var}(R_P) = R_P^{min}\sqrt{8V_{0i}/\Delta E}$, where $V_{0i} = 7$ eV is the fitted imaginary part of the inner potential describing electron attenuation. The atomic scattering for energies up to 400 eV was described by up to nine fully relativistic and spin-averaged phase shifts. They were corrected for thermal vibrations with amplitude u. For atoms in the first as well as second layers, amplitudes were allowed that were different to those applying to atoms below. We emphasize at this point that the resulting values might not strictly correspond to vibrations but could also be influenced by some compositional disorder established during (non-ideal) film growth. For the real part of the inner potential, V_{0r}, it was shown earlier that the neglect of its energy dependence—which is due to the variation of the exchange–correlation potential—can lead to systematic errors in the resulting structural parameters [18]. Thus, its energy dependence was taken into account, as described in [7]. Due to the small interlayer spacings in the silicide—a feature typical for CsCl-type and bcc(111) surfaces—the scattering properties of the whole silicide layer were described in spherical wave representation as a composite layer. The latter was stacked to the Si substrate by the layer-doubling scheme [19].

Six different atomic configurations at the interface must be considered as potential candidates, as shown in figure 2. They can be classified by (i) the coordination of the Fe atom nearest to the interface and (ii) the stacking sequence of silicide layers relative to the substrate. The coordination of Fe can be 5-, 7- or 8-fold. The stacking sequence at the interface can be unfaulted (A-type) or faulted (B-type) so that the unit cell of the silicide is oriented like that of Si or rotated by 180°, respectively. Accordingly, the notations A5, B5, A7, B7, A8 and B8 can be used to describe the different scenarios at the interface.

The spectra of the two domains with two and three iron layers within the silicide were added incoherently since—as displayed in the STM—the lateral dimension of the domains exceeds the coherence length of the probing electrons (≈100 Å). For A5 and B5, the total thickness of domains containing two (three) ML Fe amounts to four (six) atomic layers (abbreviated 4 L and 6 L), respectively. For A7, B7, A8 and B8 the total thicknesses amount to 5 L and 7 L for the two domains in each case. For the chemical identity of the outermost atomic layer, the Si termination known from our recent LEED study of a 13 Å thick film [7] was assumed. So, six model classes were tested, with two domains of different film thicknesses applying for each. As fitting parameters, the spacings between the nine outermost layers were varied, with the notation given in figure 3. Additionally, the vibrational amplitudes mentioned and—due to the experimental uncertainty—the ratio of the domain weights were allowed to vary.

2.3. Structural results

The agreement between measured and best-fit calculated spectra of the structural models tested, as quantified by the Pendry R-factor R_P, is given in table 1. Apparently, the best-fit quality can be achieved for the B8-type interface configuration ($R_P = 0.159$). Though this configuration is in agreement with conclusions from photoelectron experiments for an Fe coverage in the monolayer regime [10], we must admit that the next best interface type (B5) with $R_P = 0.180$ and $\mathrm{var}(R_P) = 0.027$ is not outside the limits of statistical errors, i.e. it cannot be excluded safely by LEED. This is due to the fact that the only qualitative difference of the B5- and B8-type

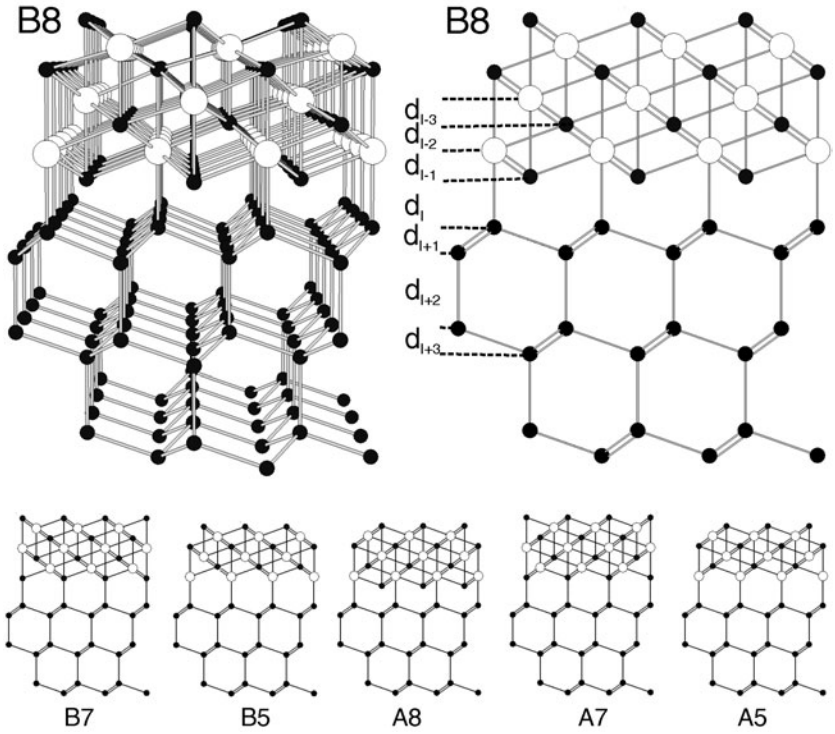

Figure 2. On the top left, the atomic arrangement in the B8 configuration of the B2-FeSi/Si(111) interface is displayed from a side-view perspective. It is repeated schematically on the right, with the notation for the first few interlayer spacings around the interface given in accordance with figure 3 and table 2. The schematic representation is also used to illustrate the other possible interface configurations, as given in the bottom panels. Large white balls represent iron atoms; small black balls correspond to silicon.

Table 1. Best-fit Pendry R-factors R_P for the different models tested. The best-fit R-factor variance amounts to $\mathrm{var}(R_P) = 0.027$.

Configuration	A5	B5	A7	B7	A8	B8
R_P	0.237	0.180	0.209	0.206	0.221	0.159

interface is the missing Si layer between the lowest Fe layer and the Si substrate (figure 2). As Si is a considerably weaker scatterer than Fe and as the layer's contribution is weakened by electron attenuation, only moderate differences can be expected for the diffraction intensities of the two models. Nevertheless, the B8-type interface provides the best fit and (except for B5) all other configurations can be ruled out. We will see below, however, that the remaining uncertainty regarding the B5 configuration can be resolved by DFT calculations. The calculated best-fit spectra are compared to the experimental data in figure 4 for two selected beams.

The best-fit parameters resulting from the best-fit model (B8) are given in part (a) of table 2 (for comparison, interlayer spacings for a thick silicide film according to recent LEED work [7] are given in part (b)). According to the LEED analysis, 50% of the silicide consists of a five-atomic-layer film (hosting 2 ML of Fe) and 50% of a seven-atomic-layer film (hosting 3 ML of Fe). Since the corresponding error is about 20%, this is equivalent to an initial coverage of 2.5 ± 0.2 ML Fe, which compares favourably with the values obtained through

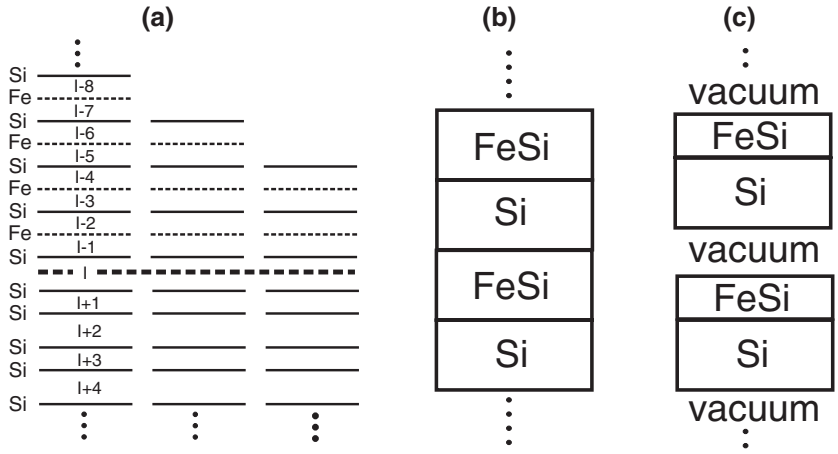

Figure 3. (a) The notation for the interlayer spacings $d_{I\pm k}$ of B2-FeSi for a very thick film (left) and a seven-atomic-layer (7 L, middle) and five-layer (5 L, right) ultra-thin film. The thick dashed line indicates the interface. Diagram (b) displays schematically a superlattice of alternating FeSi and Si blocks used in the DFT calculations in section 3.2. Diagram (c) is the same as (b) allowing, however, additionally for free silicide surfaces (section 3.3).

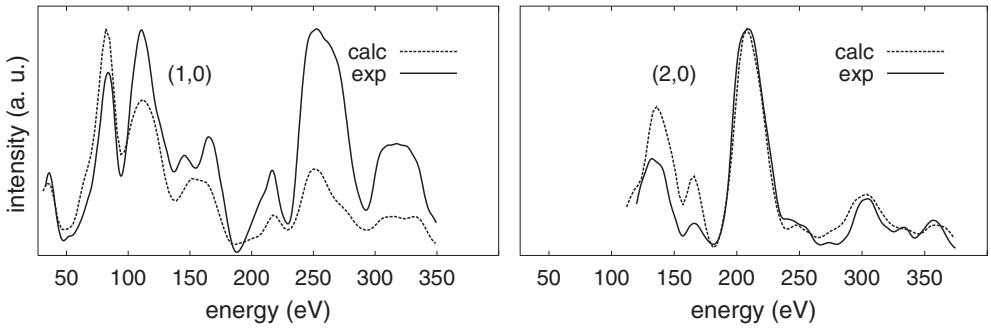

Figure 4. A comparison of calculated best-fit LEED spectra to experimental data for two selected beams.

the quartz balance (2.6 ± 0.25 ML) and the STM image evaluation (2.4 ± 0.15 ML). The layer spacings (for notation, see figures 2 and 3) exhibit large relaxations in both domains. Within the silicide film ($d_{I-6}, \ldots, d_{I-1}$) they differ by more than 0.5 Å, which is a rather high fraction of (hypothetical) B2-FeSi's bulk spacing of 0.80 Å, calculated to match the substrate's lateral unit cell (see sections 3.2). Note that spacings which have the same depth from the surface in the 5 L and 7 L domains are rather different. This holds in particular for the second and third spacings (d_{I-3} versus d_{I-5} and d_{I-2} versus d_{I-4}, respectively). The comparison with the relaxation of the surface region of a 13 Å thick silicide film [7]—which may be taken as a reference which is largely free of interface effects—also shows considerable deviations, especially for the 5 L domain. Both features indicate that there is a considerable structural interplay between the surface and the interface. Not surprisingly, therefore, the spacings at the interface (d_I) are also different for the two domains (1.57 and 1.52 Å). The Fe–Si bond lengths calculated from the spacings are 2.32 and 2.38 Å, respectively, i.e. there is only a slight contraction with respect to the bond length in bulk Fe–Si (2.40 Å). Seemingly, the bonding across the interface is of similar strength to that in Fe–Si bulk.

Table 2. (a) Best-fit parameters for the B8-type interface according to the notation introduced in figure 3 (the tabulated error margins neglect possible parameter correlations). The quantities u^1 and u^2 denote the vibrational amplitudes in the terminating Si layer and the Fe layer below, respectively, and u^b stands for the respective bulk value.

	5 L domain	7 L domain
d_{I-6} (Å)	—	0.86
d_{I-5} (Å)	—	0.66
d_{I-4} (Å)	0.82 ± 0.05	0.95
d_{I-3} (Å)	0.57 ± 0.03	0.71
d_{I-2} (Å)	1.08 ± 0.03	0.88
d_{I-1} (Å)	0.75 ± 0.04	0.86
d_I (Å)	1.57 ± 0.04	1.52
d_{I+1} (Å)	1.08	0.92
d_{I+2} (Å)	2.45	2.36
d_{I+3} (Å)	0.67	0.78 (fix)
d_{I+4} (Å)	2.47	2.36 (fix)
u^1 (Å)	0.16 ± 0.04	
u^2 (Å)	0.14 ± 0.03	
u^b(Fe) (Å)	0.08	
u^b(Si) (Å)	0.09	
V_{0i} (eV)	7.0	
Weight (%)	50 ± 20	50

Table 2. (b) For comparison, the surface layer spacings for a thick film of about 13 Å are given, according to our previous work [7].

B2-FeSi surface Reference [7]	
d_{12} (Å)	0.85 ± 0.04
d_{23} (Å)	0.68 ± 0.02
d_{34} (Å)	0.92 ± 0.02
d_{45} (Å)	0.78 ± 0.02
d_{56} (Å)	0.82
d_{67} (Å)	0.81
d_{78} (Å)	0.79
d_{89} (Å)	0.82

Finally, we address the issue of errors, which we have estimated within the silicide for the 5 L domain by using the variance of the R-factor and neglecting possible parameter correlations (similar estimations should hold for the 7 ML domain). The error for the top spacing is larger than that for deeper layers since deeper layers have smaller vibrational amplitudes u^i, thus compensating up to a certain depth the influence of electron attenuation. To shed light on the influence of parameter correlations, the latter were considered for d_I which, even for this single parameter however, requires about the same computational effort as the whole structure determination. The influence of parameter correlations turns out to be drastic, since the error limit increases from 0.04 Å (with no correlations considered) to 0.15 Å. One should keep in mind that d_I is the spacing between two Si layers which scatter less strongly than Fe layers so that, for spacings involving an Fe layer, the influence of parameter correlations might be less

pronounced. Indeed, when LEED and DFT results are compared for the same structure (see the next section) this trend can be observed. In addition, it may be possible that there is some disorder at the interface (which is not sufficiently described by the vibrational amplitude u^b), leading to an increased error.

To summarise this section, we were able to determine both the atomic configuration at the interface (B8 type) and the quantitative crystallographic structure of the film and interface. To allow a better understanding of the results, we investigate the energetics of the interface using DFT calculations, as presented in the next section.

3. Total energy calculations

3.1. Ab initio method

For the DFT calculations the Vienna *ab initio* simulation package (VASP) was applied [20], with the electron–ion interaction modelled by ultra-soft pseudo-potentials [21, 22]. Cut-off radii were 2.45 and 2.48 au for Fe and Si, respectively. The cut-off energy for the plane-wave expansion was 300 eV. The exchange–correlation functional was calculated in the generalized gradient approximation (GGA), as supplied by Perdew and Wang [23]. Since magnetism plays a role when iron-terminated FeSi slabs come into play [7], spin-polarization was allowed in all calculations. Ground states and bulk properties of the materials involved are well described within this approach [24]. The $\boldsymbol{k}$-space integrals over the Brillouin zone were approximated through summation over Monkhorst–Pack special points [25].

Different super-cell schemes were applied to compute bulk, surface and interface properties. Bulk calculations were conducted as an energy reference and to calculate epitaxial energies by adaptation to the lateral lattice parameter. The interface was described by means of a large super-cell with alternating silicide and Si blocks (equivalent to a superlattice), whereby a $7 \times 7 \times 1$ grid leading to a total of eight irreducible $\boldsymbol{k}$-points was applied. Depending on the type of interface modelled, an appropriate thickness was chosen to produce two symmetric interfaces within the super-cell, leading to blocks of FeSi and Si where at least 13 and 11 atomic layers are involved. The surface properties were calculated by introducing vacuum blocks, as usual. Since we are interested in the geometric consequences of the close proximity of the surface and the interface, an ultra-thin film was modelled by combining a five- or seven-layer B2-FeSi subblock and a 10-layer Si subblock, with a vacuum region (of $\approx$20 Å thickness) separating this combined block. We made sure that the free surface of the Si subblock is sufficiently far away from the interface to leave the latter uninfluenced. The spacings of four layers on each side of the interface and at the silicide surface were allowed to relax.

3.2. Interface energies of B2-FeSi/Si(111)

The computational treatment of the system that has been described profits largely from the information available experimentally. We take it that the film structure is of B2 type and that the shape and size of the lateral unit cell is that of the (unreconstructed) Si(111) substrate. The question remaining is which of the interface configurations is the most stable. For the Si block the (calculated) bulk lateral lattice parameter (2.728 Å) was used and B2-FeSi (bulk value: 2.770 Å) was laterally compressed to this value. To form the interface, for which the configurations A5, B5, A7, B7, A8 and B8 were again considered, the bulk materials are cleaved into blocks whereby the related energy costs represent the surface energies. The different blocks are then matched together, with a possible energy gain due to the chemical bonding. Note that—as illustrated in figure 3(b)—there are no free surfaces yet. Instead there

is a superlattice consisting of alternating FeSi and Si blocks. According to this strategy, the interface is calculated in two steps (following [26]).

First, the free (still unstrained) surfaces are formed by the cleavage of the bulk materials, yielding the surface energies E_{surf} (B2) and E_{surf} (Si). For the silicide, two values must be considered, namely those corresponding to Si and Fe termination ($B2^S$ and $B2^F$, respectively). These are derived from the differences in energies calculated for a slab/vacuum arrangement and for the bulk material. For Fe or Si termination, the FeSi slabs are non-stoichiometric, so the chemical potentials of FeSi and Si must be taken into account for calculating surface energies. Additionally, the chemical potential of the environment must be considered. This can be expressed as a deviation $\Delta\mu_{\mathrm{Si}}$ from the bulk Si chemical potential, as described in [7]. The variation of $\Delta\mu_{\mathrm{Si}}$ is limited by the existence of other stable phases and thus can vary from $\Delta H_{\mathrm{FeSi}} = -0.78$ eV (the heat of formation of FeSi—all energies are given in eV/(1 × 1) unit-cell) to zero (equivalent to the formation of elemental Si). Since the film and substrate can be assumed to be in equilibrium, $\Delta\mu_{\mathrm{Si}}$ should be close to zero. This assumption leads to surface energies $E_{surf}(B2^S, 0) = 1.13$ eV and $E_{surf}(B2^F, 0) = 2.20$ eV while, for $\Delta\mu_{\mathrm{Si}} = \Delta H_{\mathrm{FeSi}} = -0.78$ eV, the values $E_{surf}(B2^S, \Delta H_{\mathrm{FeSi}}) = 1.52$ eV and $E_{surf}(B2^F, \Delta H_{\mathrm{FeSi}}) = 1.81$ eV result. Between these limits the surface energy varies linearly as a function of $\Delta\mu_{Si}$. The surface energy of Si is $E_{surf}(\mathrm{Si}) = 1.29$ eV. All these values compare favourably with calculations using norm conserving pseudo-potentials within GGA [7].

In the second step, and to obtain the binding energy at the FeSi–Si interface, B2-FeSi and Si slabs are matched together to form a superlattice, with the common lattice parameter fixed to that of the silicon substrate so that B2-FeSi is strained. Accordingly, the slab energies E^a_{tot} are calculated for a strained slab of B2-FeSi, while silicon remains unstrained. For the superlattice, the energy $E_{tot}(B2/\mathrm{Si})$ per unit cell is calculated, whereby four layer spacings on each side of the interface were allowed to relax. The energy balance with the slab energies then yields twice the binding energy (since there are two symmetric interfaces per unit cell), i.e.

$$2E_{bind}(B2/\mathrm{Si}) = E_{tot}(B2/\mathrm{Si}) - E^{a_{\mathrm{Si}}}_{tot}(B2) - E^{a_{\mathrm{Si}}}_{tot}(\mathrm{Si}), \tag{1}$$

which, after correction by the energy costs for the formation of the free surfaces, yields

$$E_{int} = E_{bind}(B2/\mathrm{Si}) + E_{surf}(B2) + E_{surf}(\mathrm{Si}). \tag{2}$$

It should be noted that $E_{bind}(B2/\mathrm{Si})$ is independent of the strain energy, since the latter cancels in the subtraction performed in equation (1). As a consequence, this also holds for E_{int} since the surface energies are for the unstrained materials. Since for different interface models considered the FeSi blocks differ by only one silicide layer at most, the consideration of strain therefore causes just a shift of the energy zero. Equivalently, the maximum modification of E_{int} is the strain energy resulting for one layer, which is 11 meV (the energy difference between A8 and B8 would even remain constant). For the same reason, E_{int} is independent of the arbitrary thickness of the FeSi block. The resulting binding and interface energies are given in table 3. To show the dependence of E_{surf} (and, in turn, of E_{int}) on the chemical potential, the values are given for both limiting values of E_{surf}. For the case of silicide films on a thick Si substrate, $\Delta\mu_{\mathrm{Si}} = 0$ most likely describes the experimental situation. But, even for $\Delta\mu_{\mathrm{Si}} = \Delta H_{\mathrm{FeSi}}$, the stability sequence is the same. Evidently, B8 is the most stable interface configuration. However, the second most stable configuration (A8) is only 70 meV less favourable than B8. Though this value is considerably larger than thermal energy at the temperature of sample preparation (about 200–300 °C) some uncertainty might remain.

At this point we benefit from the fact that the LEED results (see table 1) could clearly exclude the A8 configuration. On the other hand, LEED could not safely rule out the B5

Table 3. Binding and interface energies (eV/unit cell) for different interface configurations.

Energies (in eV)	A5	B5	A7	B7	A8	B8
E_{Bind}	−1.71	−1.67	−1.33	−1.31	−1.72	−1.79
$E_{Int}(\Delta\mu_{\mathrm{Si}} = 0)$	1.78	1.82	1.09	1.11	0.70	0.63
$E_{Int}(\Delta\mu_{\mathrm{Si}} = \Delta H_{\mathrm{FeSi}})$	1.39	1.43	1.48	1.50	1.09	1.02

scenario for which, however, DFT shows that it is lower in energy by as much as 120 meV than the B8 type and can consequently be excluded. This is an impressive combination of the two methods: there is agreement with respect to their most favourable structures (B8), and the second best in each case can be ruled out mutually. This identifies B8 as the true configuration. An additional conclusion is that, experimentally, the equilibrium structure is assumed. As a consequence, only a single (B8-type) interface should develop in FeSi/Si heterojunctions, i.e. they should exhibit excellent lateral homogeneity. Table 4 shows that the layer spacings on both sides of the interface undergo substantial relaxations. We shall address this point in more detail in section 3.3.

It is interesting to compare the results to those for a $CoSi_2$/Si(111) interface, for which the same methods—quantitative LEED [8] and DFT [26]—have been applied. The two methods agree in identifying the 8-fold coordination, whereby LEED is in favour of B8 type and DFT in favour of A8 type (which, however, is more favourable than B8 by just 40 meV). Yet the energy differences between 8- and 7-fold coordination, as calculated by DFT, are much less pronounced for $CoSi_2$/Si(111) (60 meV [26]) than those determined in the present work for FeSi/Si(111) (about 400 meV). At first glance, this seems surprising due to the similar local structure of $CoSi_2$/Si(111), since $CoSi_2$ exhibits the CaF_2 lattice which can be constructed from B2 by taking away every second metal layer in the [111] direction. Yet it should be noted that $CoSi_2$ and B2-FeSi show pronounced differences in their bonding properties: B2-FeSi is dominated by metal–metal bonds and weaker metal–Si bonds with Si–Si bonds playing only a minor role [27], whereas $CoSi_2$ is dominated by metal–Si and Si–Si bonds of similar strength [28]. In a transition from A8 or B8 to A7 or B7, both metal–Si and Si–Si bonds change, making the quantitative outcome for both systems rather different.

Finally, we use the competition between energy gains (binding) and costs (strain) to estimate the critical number of stable B2 layers. Assuming both thermal equilibrium and flat layer-by-layer growth (for the latter we have experimental indications in the thick film regime), this is determined by

$$E_{bind}(\mathrm{B2/Si}) + n_{crit}\,E_{strain}(\mathrm{FeSi}) = 0. \tag{3}$$

With $E_{strain}(\mathrm{FeSi}) = 11$ meV/layer, a critical thickness of $n_{crit} \approx 162$ layers results, corresponding to $d_{crit} \approx 256$ Å. Of course, this holds only because B2-FeSi is a metastable and not an unstable phase. It is stabilized since, in a continuous transition from B2 → B20, the B1 phase—which is 700 meV per atom higher in energy than B2—must be overcome [24]. If the film were not metastable, it would transform into B20-FeSi at a much smaller thickness. Also, a possible gradual relaxation of strain by incorporating defects may lead to even higher film thicknesses.

3.3. Surface and interface coupling

As already mentioned, the layer spacings around the B8-type interface are considerably relaxed, as displayed in the left-hand column of table 4. Yet comparison to the above experimental results cannot be made, because the latter are for an ultra-thin silicide film with a free surface while the calculations were performed for a superlattice with no free surfaces involved

Table 4. Layer spacings around the B2-FeSi/Si(111) interface (B8 type) and at the film surfaces, as calculated by DFT and compared to the corresponding values determined by quantitative LEED. The notation of the spacings is according to figure 3(a).

Model method	Superlattice DFT	7 L film DFT	7 L film LEED	5 L film DFT	5 L film LEED
d_{I-6} (Å)	0.81 (fix)	0.85	0.86	—	—
d_{I-5} (Å)	0.81 (fix)	0.55	0.66	—	—
d_{I-4} (Å)	0.81 (fix)	1.04	0.95	0.83	0.82
d_{I-3} (Å)	0.87	0.76	0.71	0.57	0.57
d_{I-2} (Å)	0.72	0.87	0.88	1.05	1.08
d_{I-1} (Å)	0.77	0.69	0.86	0.65	0.75
d_I (Å)	1.60	1.65	1.52	1.74	1.57
d_{I+1} (Å)	0.89	0.91	0.92	0.94	1.08
d_{I+2} (Å)	2.33	2.33	2.36	2.36	2.45
d_{I+3} (Å)	0.74	0.79	0.78 (fix)	0.79	0.67

(see figure 3(b)). One should expect that for ultra-thin films the existence of a free silicide surface, i.e. the existence of truncated bonds near the interface, will modify the interface energetics and structure. To account for this requires the creation of free surfaces by the introduction of vacuum blocks, as illustrated in figure 3(c) whereby the same scheme of DFT calculations can be applied as described above. Table 4 displays the resulting computed interlayer spacings for the two experimentally identified film thicknesses (5 L and 7 L film) and compares them to the corresponding results of the LEED analysis as well as to the superlattice case. The notation of the spacings is according to figure 3(a).

The substantial relaxations at the film surfaces and at the interface, detected by both DFT and LEED, agree rather well. For the outermost three spacings in the 5 L film the agreement is within 0.03 Å. The deviations are larger for deeper layer distances and the 7 L film, yet they are still within the limits of errors estimated for the LEED results when correlations between parameters are considered (e.g. ± 0.15 Å for d_I). It should be noted that the agreement between calculated and experimental values is generally much better when spacings between Fe layers are considered. As an example, for the sum of d_{I-5} and d_{I-4} in the 7 L film—which is the spacing between the first and second subsurface iron layer—the agreement is within 0.02 Å (though the subspacings deviate by about 0.1 Å). This is due to the stronger electron scattering by Fe compared to Si.

The relaxations in the ultra-thin films are responses from the symmetry break both at the interface and the surface. It would be interesting to separate both effects, since this would allow us to obtain some information about the relaxations at deeply buried interfaces (to which LEED has no access). For a correspondingly thick silicide film ($\approx$13 Å) the surface relaxations are available [7] (see table 2). Apparently, the top three spacings—for which the influence of the interface can be considered to be negligible—are very close to the corresponding values of the 7 L film, while for the 5 L film modest agreement is only for the top spacing. Therefore, in the 7 L film the interface seems to be distant enough not to influence the surface—and vice versa. This is confirmed by the fact that the spacings at the interface calculated for a superlattice (i.e. free of surfaces) compare considerably better to those of the 7 L film than to those of the 5 L film. Each near-interface spacing of the 7 L is closer to the related superlattice spacing than to the corresponding 5 L value. This indicates that the decay length of the mutual influence of surface and interface, as carried by the strong covalent bonding in the material, is of the order of about five silicide spacings.

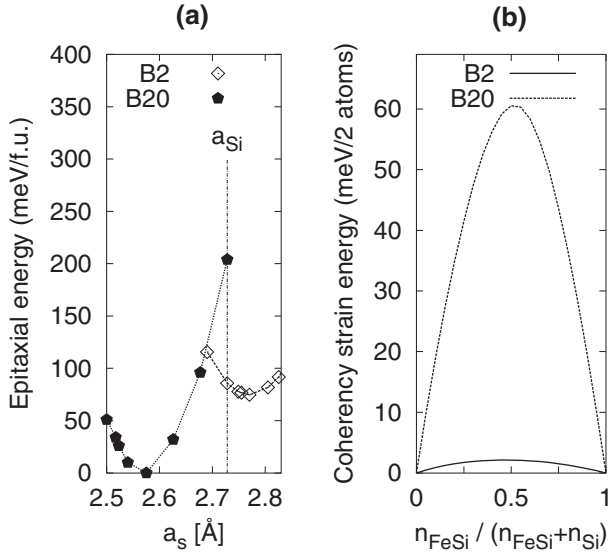

Figure 5. (a) The epitaxial energy $E_{tot}^{epi}(a_S, [111])$ for B2- and B20-FeSi as a function of the lateral lattice parameter a_S for growth in the [111] direction. At each point the vertical lattice parameter is allowed to relax. Note that, for the B20 phase, a_s must be multiplied by $\sqrt{3}$ to give the actual B20 lattice parameter. (b) The equilibrium coherency strain energy $E_{cs}^{eq}(x, [111])$ for B2- and B20-FeSi/Si(111) for a silicide/silicon superlattice as a function of the relative weight of FeSi $n_{\mathrm{FeSi}}/(n_{\mathrm{FeSi}} + n_{\mathrm{Si}})$.

3.4. Stability of epitaxial B2-FeSi film compared to the bulk phase

Though the bulk stable form of FeSi has the B20 structure (ϵ-FeSi), it is well known that high-quality B2-FeSi can grow epitaxially on Si(111) up to thicknesses of 1000 Å [4]. Thus, the energy hierarchy seems to be reversed by some epitaxial restrictions such as the enforced new lateral lattice parameter and/or the bonding at the interface. Earlier, it was claimed that only the latter makes B2-FeSi energetically favourable [9]. On the other hand, the energy difference between B2- and B20-FeSi is small, so elastic contributions can become decisive [29]. Therefore, we try to resolve this issue in the following. Also, we attempt to expand the considerations from single epitaxial films to the FeSi/Si superlattice, with arbitrary slab thicknesses of FeSi and Si.

In principle, the energy of an epitaxial film can be separated into its chemical and its strain energy. While the latter gives the energy change caused by deformation of the parent film material to the lateral substrate lattice parameter, the chemical energy includes all effects caused by the interaction of film and substrate at their interface. Certainly, for thick films the elastic energy must dominate. Thus we concentrate on that comparing B2- and B20-FeSi. For the B2 phase the matching of its (111) face to the Si(111) substrate is favourable since its lattice parameter is just 1.5% larger (2.77 versus 2.73 Å). In contrast, for B20-FeSi, structural coherency with the substrate requires a contraction of about 5%, whereby the film forms a $(\sqrt{3}\times\sqrt{3})$R30° superstructure relative to the (1×1) phase of bulk-terminated Si(111) [30, 31].

Figure 5(a) displays the epitaxial energy $E^{Epi}(a_S, \hat{G})$, which represents the energy of the film material epitaxially deformed to different lattice parameters a_S of the hexagonal substrate unit cell and allowed to relax along $\hat{G} = [111]$. This coincides with the total energy of the unstrained film materials when their equilibrium lattice parameters are assumed,

i.e. $a_{S0}(B20) = 2.57$ Å for the B20 phase and $a_{S0}(B2) = 2.77$ Å for the B2 phase (the B20 equilibrium phase defines the energy zero). With epitaxial strain imposed (i.e. with varying a_S) there is an almost parabolic variation $E^{epi}(a_S, \hat{G})$ for both phases. (It should be noted that the curvatures do not produce the bulk moduli because, for each value of a_S, the vertical lattice parameter was allowed to relax freely in order to minimize the energy under the strain imposed. The hydrostatic energy would have a considerably larger curvature.)

The energy scale in figure 5(a) is relative to the formula unit (fu), i.e. it gives the energy per pair of Fe and Si atoms. At their equilibrium lattice parameters, the B20 phase is favoured by 75 meV/f.u. over the B2 phase—a value in close agreement with earlier *ab initio* results [24, 32]. Yet, when the silicides are epitaxially forced to assume a lattice parameter larger than $a_S \approx 2.7$ Å, the situation is reversed. For epitaxial growth on Si(111), i.e. at $a_S = a_{\mathrm{Si}} = 2.728$ Å (indicated by the vertical line in figure 5(a)), the B2 phase is lower in energy by 118 meV/f.u. than B20-FeSi. One should note that this result is independent of the chemical nature of the substrate, i.e. no contributions of the bonding between the film and substrate are necessary to favour B2 over B20. This finding is at variance with an earlier study based on empirical total energy calculations [9], which leads to the conclusion that chemical energies stabilize B2-FeSi. Also, the latter method gives a much higher energy difference between B20- and B2-FeSi (540 meV) than the present study and other *ab initio* calculations [24, 32].

The results presented so far apply to the fixed substrate lattice parameter. Yet, when a superlattice of the two materials is grown, they will compromise on a new common lattice parameter that will depend on the relative weight of silicide: $x = n_{\mathrm{FeSi}}/(n_{\mathrm{FeSi}} + n_{\mathrm{Si}})$, where n denotes the number of layers of the respective material. To decide if, under the new conditions, B2-FeSi is still favoured over B20-FeSi, we use the *coherency strain energy*, E^{eq}_{cs}, i.e. the energy to maintain lateral coherency between FeSi and Si orthogonal to the direction of growth, $\hat{G}$. For large values of both n_{FeSi} and n_{Si} corresponding to an infinite superlattice period, interfacial interactions between FeSi and Si are again negligible, i.e. only elastic energies remain. In this case, the competition between the epitaxial strain energies of FeSi and Si determines the equilibrium lateral lattice parameter a_p, equivalent to

$$E^{eq}_{cs}(x, \hat{G}) = \min_{a_p}[x E^{epi}_{\mathrm{FeSi}}(a_p, \hat{G}) + (1 - x) E^{epi}_{\mathrm{Si}}(a_p, \hat{G})] \tag{4}$$

whereby the minimization with respect to a_p includes the full relaxation of the vertical lattice parameters c in the two materials (already included in the epitaxial energies). The quantity $E^{eq}_{cs}(x, \hat{G})$ is displayed in figure 5(b), which tells us that the B2-FeSi phase is favoured over B20-FeSi, independently of the ratio x. Therefore, even when Si responds to the strain of growing FeSi, elasticity favours B2-FeSi, which will consequently be realized in any FeSi–Si superlattice.

Up to this point we have not considered the chemical energy (i.e. the bonding of the two materials at their interface). Yet it will not reverse the energetic hierarchy found above, since the B20-Si(111) interface cannot avoid dangling bonds [9] and therefore cannot be more stable than B2-FeSi, in agreement with the latter's growth observed by experiment.

4. Conclusion

We have demonstrated the growth of ultra-thin B2-FeSi films on Si(111) with good crystalline quality and a sharp interface through deposition of about 2.5 ML Fe and subsequent annealing. The best fit of the LEED structure analysis corresponds to the B8-type interface, i.e. the Fe atom next to the substrate is coordinated by eight Si atoms, with the stacking of FeSi layers

reversed compared to Si (B type). Yet, while all other bonding scenarios (A5, A7, B7, A8) can be ruled out, the B5 configuration is not outside the limits of errors. Using DFT calculations based on GGA and ultra-soft pseudo-potentials, we calculated the stability of different interface structures. Indeed, the B8 configuration turns out to be the most stable one, 70 meV lower in energy than the A8 type. Though this value is larger than the thermal energy at the temperature of measurement, some uncertainty might remain. Yet the A8 configuration is clearly ruled out by LEED. DFT rewards us by clearly excluding the B5 type, which LEED could not safely rule out. So, through joint application of the two methods, the B8 configuration is clearly identified.

The layer spacings—both at the interface and the surface of the film—show substantial relaxations, whereby DFT and LEED agree within the latter's limits of errors. For silicide films about five layers thick or thinner, the film surface and interface influence each other substantially. Comparison of the B2 phase with the bulk-stable B20 phase of FeSi shows that it is the epitaxial strain that makes B2-FeSi/Si(1111) more stable than B20-FeSi/Si(111). This holds even when, in the FeSi/Si superlattice, both the constituent FeSi and Si slabs are allowed to relax to a common lateral lattice parameter.

Acknowledgments

We would like to thank R Podloucky (Vienna) for helpful discussions. Financial support from the Deutsche Forschungsgemeinschaft (DFG) is also gratefully acknowledged.

References

[1] Lange K 1997 *Phys. Status Solidi* b **201** 3
[2] Leong D N, Harry M, Reeson K J and Homewood K P 1997 *Nature* **387** 686
[3] Pauling L and Soldate A M 1948 *Acta Crystallogr.* **1** 212
[4] von Känel H, Mäder K A, Müller E, Onda N and Sirringhaus H 1992 *Phys. Rev.* B **45** 13807
[5] Hinarejos J J, Castro G R, Segovia P, Alvarez J, Michel E G, Miranda R, Rodríguez-Marco A, Sánchez-Portal D, Artacho E, Ynduráin F, Yang S, Ordejón P and Adams J B 1997 *Phys. Rev.* B **55** 16065
[6] Starke U, Weiss W, Kutschera M, Bandorf R and Heinz K 2002 *J. Appl. Phys.* **91** 6154
[7] Walter S, Bandorf R, Weiss W, Starke U, Heinz K, Strass M, Bockstedte M and Pankratov O 2003 *Phys. Rev.* B **67** 085413
[8] Seubert A, Schardt J, Weiß W, Starke U and Heinz K 2000 *Appl. Phys. Lett.* **76** 727
[9] von Känel H, Schwarz C, Gonvalves-Conto S, Müller E, Miglio L, Tavazza F and Malegori G 1995 *Phys. Rev. Lett.* **74** 1163
[10] Mascaraque A, Avila J, Teodorescu C, Asensio M C and Michel E G 1997 *Phys. Rev.* B **55** R7315
[11] Heinz K 1995 *Rep. Prog. Phys.* **58** 637
[12] Blum V and Heinz K 2001 *Comput. Phys. Commun.* **134** 392
[13] Rous P J, Pendry J B, Saldin D K, Heinz K, Müller K and Bickel N 1986 *Phys. Rev. Lett.* **57** 2951
[14] Rous P J and Pendry J B 1989 *Surf. Sci.* **219** 355
Rous P J and Pendry J B 1989 *Surf. Sci.* **219** 373
[15] Rous P J 1992 *Prog. Surf. Sci.* **39** 3
[16] Kottcke M and Heinz K 1996 *Surf. Sci.* **376** 352
[17] Pendry J B 1980 *J. Phys. C: Solid State Phys.* **13** 937
[18] Walter S, Blum V, Hammer L, Müller S, Giesen M and Heinz K 2000 *Surf. Sci.* **458** 155
[19] Pendry J B 1974 *Low-Energy Electron Diffraction* (London: Academic)
[20] Kresse G and Furthmüller J 1996 *Comput. Mater. Sci.* **6** 15
Kresse G and Furthmüller J 1996 *Phys. Rev.* B **54** 11169
[21] Vanderbilt D 1990 *Phys. Rev.* B **41** 7892
[22] Kresse G and Hafner J 1994 *J. Phys.: Condens. Matter* **6** 8245
[23] Perdew J P and Wang Y 1992 *Phys. Rev.* B **45** 13244 and references therein
[24] Moroni E G, Wolf W, Hafner J and Podloucky R 1999 *Phys. Rev.* B **59** 12860

[25] Monkhorst H J and Pack J D 1976 *Phys. Rev.* B **13** 5188
[26] Stadler R, Vogtenhuber D and Podloucky R 1999 *Phys. Rev.* B **60** 17112
[27] Mäder K A, von Känel H and Baldereschi A 1993 *Phys. Rev.* B **48** 4364
[28] Stadler R, Podloucky R, Kresse G and Hafner J 1998 *Phys. Rev.* B **57** 4088
[29] Moroni E G, Hafner J and Podloucky R 1998 *Phys. Rev. Lett.* **81** 1969
[30] von Känel H, Onda N, Sirringhaus H, Müller-Gubler E, Goncalves-Conto S and Schwarz C 1993 *Appl. Surf. Sci.* **70/71** 559
[31] Hinarejos J J, Segovia P, Alvarez J, Castro G R, Michel E G and Miranda R 1998 *Phys. Rev.* B **57** 1414
[32] Al-Sharif A I, Abu-Jafar M and Qteish A 2001 *J. Phys.: Condens. Matter* **13** 2807